AGU PUBLICATIONS

Geophysical Research Letters

RESEARCH LETTER
10.1002/2015GL064576

Key Points:
- Spatiotemporal map of the surface deformation associated with Lusi mud eruption
- Time-dependent source model of the Lusi and nearby gas field
- Revealing the deep and shallow sources of the Lusi and characterizing their relationship

Supporting Information:
- Movie S1
- Texts S1–S4, Figures S1–S12, and Tables S1 and S2

Correspondence to:
M. Shirzaei,
shirzaei@asu.edu

Citation:
Shirzaei, M., M. L. Rudolph, and M. Manga (2015), Deep and shallow sources for the Lusi mud eruption revealed by surface deformation, *Geophys. Res. Lett.*, *42*, 5274–5281, doi:10.1002/2015GL064576.

Received 15 MAY 2015
Accepted 23 JUN 2015
Accepted article online 25 JUN 2015
Published online 14 JUL 2015

Deep and shallow sources for the Lusi mud eruption revealed by surface deformation

Manoochehr Shirzaei[1], Maxwell L. Rudolph[2], and Michael Manga[3]

[1]School of Earth and Space Exploration, Arizona State University, Tempe, Arizona, USA, [2]Department of Geology, Portland State University, Portland, Oregon, USA, [3]Department of Earth and Planetary Science, University of California, Berkeley, California, USA

Abstract The Lusi mud eruption, in East Java, Indonesia, began in May 2006 and continues to the present. Previous analyses of surface deformation data suggested an exponential decay of the pressure in the mud source but did not constrain the location, geometry, and evolution of the possible source(s) of the erupting mud and fluids. To map the surface deformation, we employ multitemporal interferometric synthetic aperture radar and analyze a well-populated L-band data set acquired by the Advanced Land Observing Satellite (ALOS) between May 2006 and April 2011. We then apply a time-dependent inverse modeling scheme. Volume changes occur in two regions beneath Lusi, at 0.3–2.0 km and 3.5–4.75 km depth. The cumulative volume change within the shallow source is ~2–3 times larger than that of the deep source. The observation and model suggest that a shallow source plays a key role by supplying the erupting mud, but that additional fluids do ascend from depths >4 km on eruptive timescales.

1. Introduction

The Lusi mud eruption began on 29 May 2006 and continues to erupt at present. The eruption has caused >$4 billion in economic losses and displaced more than 60,000 people from their homes [*Richards*, 2011]. It is also the largest historical subaerial mud eruption.

Models to interpret the history, and predict the future, of the eruption require understanding several features of the subsurface. Because the eruption began approximately 200 m [*Istadi et al*., 2009] away from a gas exploration well (Banjar-Panji 1, hereafter BJP-1), the subsurface lithology and petrophysical properties were characterized prior to the initiation of the eruption. However, the sources of erupting fluids, the timing of their syneruptive or preeruptive ascent, and the importance of overpressure in the individual mud and fluid sources are less certain. Measurements of ground deformation, resulting from the withdrawal of mud and fluids from the subsurface, in combination with inverse source modeling approaches, have the potential to better constrain the locations of mud and fluid sources and their evolution during the eruption.

The material erupting from Lusi contains water (liquid and steam), noncondensable gases, and solid particles. Identifying the source(s) of each component of the erupting material is key to understanding the processes that drive the eruption as well as those that may have initiated the eruption. There are a variety of geochemical constraints on the source of solids, gas, and water and their variations over time. The clay mineralogy, dominantly illite with some chlorite [*Mazzini et al*., 2007], is consistent with a primary mud source at 1615–1828 m depth with secondary contributions from more shallow sources between 1341 and 1432 m [*Mazzini et al*., 2007]. Erupted gases measured at BJP-1, however, suggest that the initial eruption (first day) expelled fluids from greater depths. The erupting mud is at or very near the boiling point, and a temperature of 100°C was reached at 1700 m depth in BJP-1 [*Mazzini et al*., 2007]. The composition of the gaseous phase is dominantly water vapor (>96%) based on measurements performed in October 2011 [*Vanderkluysen et al*., 2014]. $^3He/^4He$ ratios of samples collected in 2010–2011 imply a significant mantle or magmatic contribution [*Mazzini et al*., 2012] and hence a deeper source of fluid. C isotopes in CO_2 and CH_4 indicate CO_2-CH_4 equilibration at high temperatures (>200°C), consistent with production at depths >4 km. Mixing of fluid sources may not be simple: CO_2/CH_4 varies by a factor of a few over short time periods [*Vanderkluysen et al*., 2014] but shows no obvious systematic trends over time [*Mazzini et al*., 2007, 2012]. The erupting mud reportedly had a water content of 60 vol % initially, decreasing to 30 vol % in June 2007 [*Mazzini et al*., 2007], though subject to considerable uncertainty (A. Mazzini, personal communication, 2014). This implies that the relative contributions of mud and fluid sources may have changed over the course of the eruption.

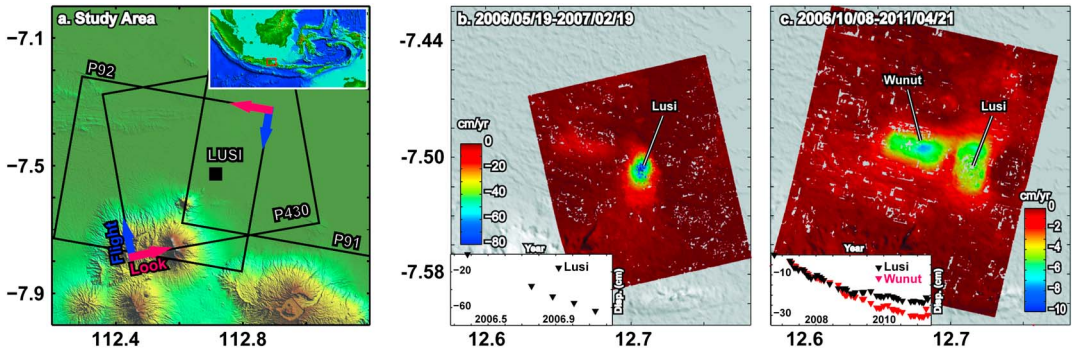

Figure 1. (a) Study area and the shaded relief (Shuttle Radar Topography Mission). Black boxes show SAR data footprint. Inset shows Java and Sumatra and location of Lusi. (b) LOS velocity field spanning the early stage of the eruption. The SAR geometry is ascending with heading and incidence angles of ~350° and ~49°, respectively. Inset shows cumulative LOS displacement at Lusi. (c) LOS velocity field spanning the latter stage of the eruption. The SAR geometry is descending with heading and incidence angles of ~190° and ~38°, respectively. Inset shows cumulative LOS displacement at Lusi and Wunut.

We present a new analysis of ground deformation with the objective of constraining the source of erupted materials. Previous studies of ground deformation at Lusi using interferometric synthetic aperture radar (InSAR) documented subsidence in the area around the vent [*Abidin et al.*, 2009]. The overall rate of subsidence between 2007 and 2011 decreased exponentially in time with a characteristic decay time of ~2 years [*Rudolph et al.*, 2013; *Aoki and Sidiq*, 2014]. Here we use multitemporal interferometric processing of L-band synthetic aperture radar (InSAR) data acquired by the ALOS satellite between 2006 and 2011. We then apply a time-dependent inversion procedure to identify three distinct sources that in combination explain the observed spatial and temporal pattern of ground deformation. We quantify the volume changes associated with each source and how the contributions of the different sources changed during the first 6 years of the eruption.

2. Data and Methods

2.1. Multitemporal InSAR

To generate the time series of the surface deformation, we employ a multitemporal SAR interferometry approach [*Shirzaei*, 2013]. The data set includes SAR images acquired by the ALOS L-band satellite from May 2006 to April 2011 and includes 5 scenes in the ascending orbit track frame 430 and 21 and 23 scenes in the descending orbit tracks frames 21 and 25, respectively (Figure 1a and Table S1 in the supporting information). Using these data, we generated ~420 interferograms. The geometrical phase is estimated and subtracted using satellite ephemeris data and a reference Shuttle Radar Topography Mission [*Farr et al.*, 2007] digital elevation model with 90 m horizontal resolution [*Massonnet et al.*, 1993; *Franceschetti and Lanari*, 1999]. To obtain an unambiguous range displacement from modulo 2π phase change measured in each interferogram, we use a 2-D phase unwrapping operator [*Chen and Zebker*, 2001]. This operator is applied to a sparse network of stable pixels [*Costantini and Rosen*, 1999]. For details on the elite (i.e., less noisy) pixel selection, see *Shirzaei* [2013]. The effect of satellite orbital error in each unwrapped interferogram is reduced following the method proposed by *Shirzaei and Walter* [2011]. We also corrected every interferogram for spatially correlated components of the atmospheric delay [*Shirzaei and Bürgmann*, 2012]. This data set is then inverted using a linear unbiased estimation approach [*Bjerhammar*, 1973] to generate a time series of the surface deformation. High-pass filtering in space and low-pass filtering in time are applied to reduce the atmospheric delay. The line-of-sight (LOS) displacement rate of each pixel is estimated as the slope of a best fitting line to the displacement time series using a robust regression approach.

2.2. Time-Dependent Source Inversion

To investigate the source of the observed surface deformation, we employ an inverse source modeling scheme. We introduce a regular 3-D grid of point centers of dilatation (PCD) at locations $\{X_i, Y, Z_i\}$ buried in a homogenous isotropic elastic half-space and solve for the volume change $dv(X_i, Y, Z_i), i = 1, 2, ..., m$

associated with each PCD [*Mossop and Segall*, 1999; *Vasco et al*., 2002]. A PCD uses elastic half-space Green's functions and consists of three mutually orthogonal double forces [*Segall*, 2010]. Variations of this method were used to study volume change distribution underneath Long Valley Caldera [*Vasco et al*., 1988], to estimate volumetric strain at the Geysers geothermal field [*Mossop and Segall*, 1999], to constrain pressure changes underneath volcanoes on Seguam Island, Alaska [*Masterlark and Lu*, 2004], and to investigate spatiotemporal distribution of volumetric strain underneath Camp Flegrei volcano, Italy [*D'auria et al*., 2012]. The PCD solution that we employ does not allow for nonlinear response of the subsurface, including brittle faulting, plastic deformation, or finite-strain elasticity. However, the strains calculated using our inverse model are $O(10^{-5})$, significantly smaller than the threshold of $O(10^{-3})$ typically used as an upper limit for linear elasticity.

The modeling approach applied here is identical to that of *Masterlark and Lu* [2004], except that we solve for the volume change distribution of PCDs rather than pressure change associated with distributed pressurized spherical sources. We do not use pressurized spherical sources, because the pressure change in the vicinity of each pressurized source is affected by stress imparted by the other sources [*Pascal et al*., 2014], and thus, its interpretation "is not well motivated on physical grounds" [*Segall*, 2010]. Because of this well-known limitation of the application of multiple PCDs to the problem of volcano deformation source modeling, we do not attempt to relate the volume changes recovered from our inverse model to pressure changes.

To invert for the volume change distribution $dv(X_i, Y_i, Z_i)$, $i = 1, 2, ..., m$, in an elastic half-space from the observed LOS surface deformation $L = [L_1, L_2, \ldots, L_n]^T$ we solve

$$\begin{bmatrix} L_1 \\ . \\ . \\ . \\ L_n \end{bmatrix} = \begin{bmatrix} G_1 & \ldots & G_m \end{bmatrix} \begin{bmatrix} dv_1 \\ . \\ . \\ . \\ dv_m \end{bmatrix} + \begin{bmatrix} r_1 \\ . \\ . \\ . \\ r_n \end{bmatrix}, \tag{1}$$

where G includes the PCD elastic Green functions and the LOS unit vectors and r is observation residual. The total volume change associated with the distribution of PCDs is obtained following

$$dV = \sum_{i=1}^{m} dv_i = \frac{\iint_{R^2} L \, dx dy}{2(1-\vartheta)c_z} \tag{2}$$

where c_z is the unit vector projecting the vertical deformation onto the LOS (see supporting information for details). To avoid the unrealistic variations of the volume changes, we minimize the second derivative of the volume changes [*Harris and Segall*, 1987]. Equation (1) is solved by minimizing the L1 norm of the residuals. The advantage of the L1 norm over the more widely used L2 norm is that it is less sensitive to outliers and thus reduces their impact on the estimated parameters [*Marshall and Bethel*, 1996]. To determine the temporal evolution of the volume change, we additionally use a linear Kalman filter [*Grewal and Andrews*, 2001] to generate time series of the volume change for each PCDs [*Shirzaei and Walter*, 2010].

To demonstrate the effectiveness of this inversion method, we present results from several synthetic tests (Figures S1–S4) in which we invert simulated surface deformation (with 10% added random noise) using the methods described in this section. Within these tests we simulated the surface deformation due to opening of a sill (Figure S1), inflation of an ellipsoid (Figure S2), a torus (Figure S3), and two adjacent spheres (Figure S4). The details of the synthetic tests as well as the model setup are given in Table S2. We then use the inversion scheme presented here (equation (1)) to solve for the distributed volume change associated with each of simulated surface deformation fields. The tests show that this method is able to accurately resolve the location and amplitude of the volume changes associated with different source settings. The errors in the inverted volume changes are 3.7%, 4.5%, 3.7%, and 4.4%, respectively, for sill, ellipsoid, torus, and two adjacent spheres.

To investigate the source of the deformation field at Lusi, we consider a 3-D array of the PCDs with 1 km and 0.2 km of horizontal and vertical spacing, respectively, for a total of 3375 PCDs. We tested the model resolution, including the density of PCDs, as well as the effects of the observation gap and estimated noise on the resolved volume change distribution, described in detail in the supporting information.

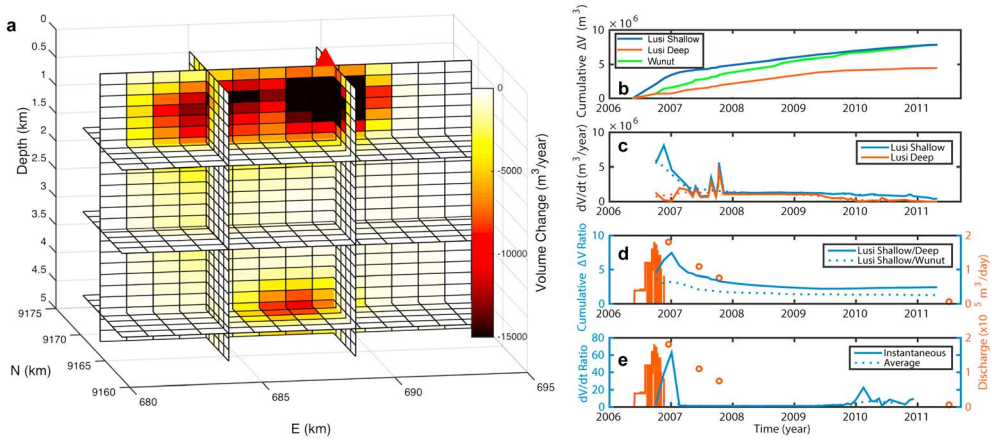

Figure 2. Model results. (a) Slice plot shows the 3-D distribution of the volume change rate averaged over the duration of the study. Coordinates are reported in UTM (Universal Transverse Mercator), zone 49 (corresponding to 112.6316–112.7670 E and 7.4601–7.5962 S). (b) Cumulative volume changes associated with the shallow (blue) and deep (red) sources beneath Lusi and Wunut (green) and (c) rate of volume change within the shallow (blue) and deep (red) sources. Solid lines show instantaneous values while dotted lines show a 6 month average. (d) Ratios of cumulative volume change. Solid line indicates the ratio between the shallow and deep sources beneath Lusi, while dotted line indicates the ratio of Lusi shallow and Wunut sources, and (e) ratios of rate of volumetric change in shallow and deep sources beneath Lusi. Solid line indicates instantaneous ratio while dotted line indicates a 6 month average. In Figures 2d and 2e, we show discharge measurements compiled from *Mazzini et al.* [2007, 2009, 2012].

3. Results

Figures 1b and 1c show the LOS velocity fields obtained following multitemporal analysis of the ascending and descending SAR data sets. The ascending data set (Figure 1b) covers the early stage of the eruption, spanning 19 May 2006 to 17 February 2007, and reveals up to 80 cm/yr of LOS subsidence. The inset in Figure 1b shows the time series of the cumulative surface displacement within the first 9 months, which indicates steady subsidence. Figure 1c presents the LOS displacement velocity for the period 8 October 2006 to 21 April 2011. This map reveals two regions of subsidence at rates of up to ~10 cm/yr. In Figure 1c, the signal to the east is associated with Lusi, while the one to the west is related to Wunut gas field, located ~5 km west of Lusi. The inset shows the time series of the cumulative LOS subsidence at Lusi and Wunut, both characterized by an exponential decay. As shown here, the rate of subsidence at Wunut is not constant and increases toward end of the period. Nonetheless, it is not clear whether this increase is in response to the Lusi eruption.

The inversion results (Figure 2a and supporting information Movie S1) show that the spatiotemporal deformation field is well explained using a combination of three deflating zones: the first at 0.3–2.0 km depth beneath Lusi, the second at similar depth beneath Wunut, and the third at 3.5–4.75 km beneath Lusi (Figure 2a). The shallow source underneath Lusi corresponds to those obtained in earlier studies [*Fukushima et al.*, 2009]. The spatial distribution of these sources is stationary throughout the observation period (see supporting information Movie S1) and the total volume changes are 8.8×10^6 m^3, 4.4×10^6 m^3, and 6.3×10^6 m^3, respectively. Through error propagation [*Mikhail*, 1976], we obtained the standard deviation of the volume change distribution (Figure S7a). We also provided the error bars on the cumulative volume change at 99% confidence interval. The error analysis and confidence intervals suggest that inversion results are robust and the difference between shallow and deep sources is statistically significant.

During the first months of the eruption, the volume change in the shallow source beneath Lusi is 4.5 times larger than that of the deeper one. This ratio increases to 7 by the beginning 2007. It then gradually decays, and toward the end of the study period the ratio drops to a factor of 2 (Figure 2d). While the ratio of the volume change within the shallow source beneath Lusi to that of the Wunut source is high (~3) initially, it decays exponentially until it drops to about 1 (Figure 2d). The time series of the volume change ratio and the error bars at 99% confidence interval are provided in Figure S7c. The histograms of the model misfits associated with the time-dependent source inversion are shown in Figure S6.

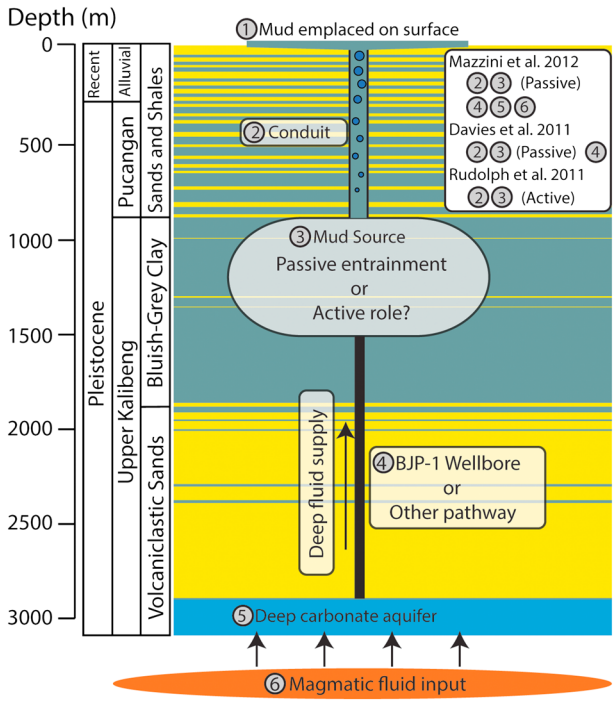

Figure 3. Schematic illustration of mud and fluid sources and conduits sustaining Lusi. Each component of the conceptual model is numbered and discussed in the text. The inset legend lists the components present in three conceptual models for Lusi.

4. Discussion

4.1. Fluid Sources

The depth of the inferred shallow source beneath Lusi is consistent with earlier estimates using deformation data and source modeling [*Fukushima et al.*, 2009] and inferences based on gas measurements, temperature, microfossils, and kerogen compositions from sidewall cores in BJP-1 [*Mazzini et al.*, 2012]. We also resolve deformation from deep sources (3.5–4.75 km). A deep source of fluids during the initiation of the eruption is consistent with the gas geochemistry measured during the first days of the eruption at the BJP-1 well. The centroid of the cumulative volumetric change associated with this source is at 4350 m depth (Figure S8). *Mazzini et al.* [2012] argue, based on $\delta^{13}C$ of hydrocarbons, that the gas source after 2006 was deeper than the mud source and most likely came from a marine source rock, possibly marine shales in the Ngimbang Formation at depths >4400 m, consistent with our deep reservoir. Previous studies have suggested that some of the erupting water comes from a carbonate aquifer around 2.8 km depth [*Tingay et al.*, 2008; *Istadi et al.*, 2009; *Davies et al.*, 2011], likely in the Middle Miocene Tuban Formation, which was reached or nearly reached by BJP-1 [*Tingay*, 2015]. We see no geodetic evidence for significant volumetric deformation sources at this depth. However, detection of H_2S associated with the kick in BJP-1 preceding the eruption, together with the fact that the Miocene carbonates are the only known source of H_2S in the East Java Basin, is a strong indication that some fluids were removed from this depth during the initial phase of the eruption [*Tingay et al.*, 2015].

The water content of the erupting mud reportedly ranged from 30 to 60 vol %. While the erupting mud's water content decreased, the discharge from Lusi increased from ~4×10^4 m^3/d in June–July 2006 to 1.8×10^5 m^3/d in late September 2006 [*Mazzini et al.*, 2007]. Thus, during this period, the viscosity of erupting mud, which is strongly affected by water content [*Rudolph and Manga*, 2010], was not the primary control on discharge. Rather, discharge was likely affected by changes in conduit geometry. In Figure 2e, we compare the ratio of volume change rates in the shallow and deep sources beneath Lusi with discharge measurements. Coincident with the increased discharge in late 2006, we find increasing relative contribution from the shallow source. Increased discharge in late 2007 likely reflects primarily an increased mixing ratio of mud derived from the shallow source with a constant supply of fluids derived from deeper sources (Figures 2c and 2d). A reanalysis of the petrophysical logs from BJP-1 found density of 2.0 g/cm^3 and porosity of 40–50% throughout the Upper Kalibeng Formation (UKF hereafter) [*Lupi et al.*, 2014; *Tingay*, 2015]. Thus, based on the measured density and porosity estimates in the inferred mud source, little or no additional water may be necessary to match the water content of the erupting mud after the initial water-rich phase of the eruption.

We calculated the ratio of cumulative volumetric change in the deep source to that in the shallow source (Figure 2d) as well as the ratio of rates of volumetric change in the shallow and deep sources (Figure 2e). The mixing ratio of shallow- to deep-sourced material varied between ~1 and 62, increasing through early 2007, then decreasing, and has been nearly constant since 2009.

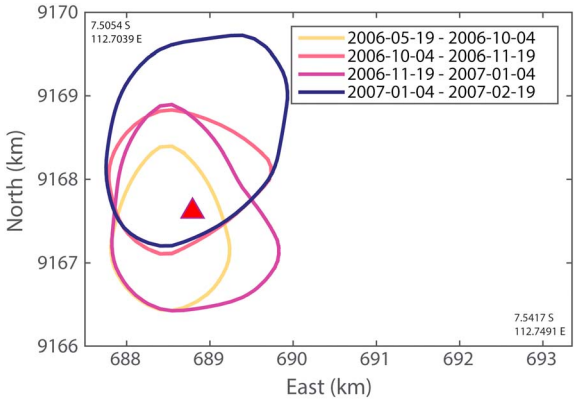

Figure 4. Vertically integrated rate of volumetric change above 2500 m depth beneath Lusi (red triangle) between May 2006 and April 2007. The contours indicate a proxy for the lateral extent of the mud chamber (described in text). Axes are reported in UTM (zone 49).

4.2. Conceptual Models for Lusi

Three conceptual models have been proposed for Lusi. Figure 3 shows the components (numbered) included in all models, though not all components are present in every model. In the model of *Davies et al.* [2011], used to predict longevity, two distinct sources of mud and fluids sustain the eruption. Water is expelled from a deep aquifer (component 5), flows upward (initially) through the wellbore of BJP-1 (4), entrains mud passively (3), and ascends to the surface through hydrofractures initiated at or below the casing shoe of BJP-1. The eruption is sustained by overpressure in the aquifer, and the longevity of the eruption is determined by the rate of pore pressure decrease in a saturated, confined aquifer. *Davies et al.* [2011] predicted that the eruption is likely to last more than 26 years, though discharge is expected to decrease exponentially. In the second conceptual model [*Rudolph et al.*, 2011], the eruption is sustained by overpressure within the mud source (3) in the UKF and by the exsolution and expansion of gas as it ascends through a conduit (2) that may have initially been composed of hydrofractures, as in the model by *Davies et al.* [2011]. *Rudolph et al.* [2011] argued that because the erupting mud had water content of ~30% after the initial water-rich phase, consistent with estimates of porosity in the UKF, little or no additional fluid was added. The mud in the UKF would be progressively mobilized over the course of the eruption as the evacuation of material from a "mud chamber" concentrated elastic stresses in the surroundings. In this model, the eruption might terminate due to decreasing pressure in the mud source, or alternatively the eruption might culminate in the formation of a caldera, having approximately the same lateral dimension as the mobilized region of mud at depth. The model by *Rudolph et al.* [2011] was used to make a probabilistic longevity prediction, arriving at a similar conclusion to *Davies et al.* [2011], primarily because both models used discharge as a constraint on the values of free parameters. The third conceptual model by *Mazzini et al.* [2012] is based on an extensive suite of fluid and gas geochemical observations using samples obtained between the initiation of the eruption and 2011. *Mazzini et al.* [2012] find evidence early in the eruption for biogenic methane from shallow depths (only in the early stages of the eruption in 2006). While *Mazzini et al.* [2012] did not predict longevity, they suggested that longevity would be controlled by the accumulation of overpressure in the hydrothermal system feeding Lusi and its release by the ongoing eruption, which may be affected by deformation along the Watukosek Fault.

Of the conceptual models presented, the model by *Mazzini et al.* [2012] is most consistent with the sources of deformation inferred here. We find evidence for significant volumetric changes in the shallow mud source (component 3 in Figure 3) as well as the deep source, whose centroid depth coincides with the source of hydrocarbons emitted at Lusi proposed by *Mazzini et al.* [2012]. We resolve temporal variations in the ratio of volume fluxes from the shallow and deep source regions, implying that the simple entrainment model (assuming constant volumetric mixing ratio between water and mud) used by *Davies et al.* [2011] may not be applicable to Lusi. A deep fluid source was not considered in the conceptual model of *Rudolph et al.* [2011] because the water content of the erupting mud since late 2006 has been comparable to the porosity in the mud source region [*Mazzini et al.*, 2007]. Two aspects of the conceptual model of *Rudolph et al.* [2011] that remain relevant are (1) the possibility that the mud source has expanded laterally during the course of the eruption and (2) the possibility that the eruption will culminate in the formation of a caldera. In Figure 4, we show the vertically integrated volumetric change associated with the mud source beneath Lusi in 2006–2007. We show contours delineating the surface along which the rate of volumetric change is one third the maximum value, a proxy for the lateral extent of the mud reservoir. Volumetric change is initially restricted to a relatively small region around the vent location (indicated with red triangle). Between late 2006 and early 2007, the mud source grew laterally. As long as mud continues to be removed from the shallow reservoir feeding Lusi, elastic stresses will increase in the surroundings, and a caldera or collapse feature similar to the nearby Porong collapse structure [*Kusumastuti et al.*, 2002] could form.

5. Conclusions

We produced a new spatiotemporal record of ground deformation near Lusi using InSAR. We subsequently modeled the observed ground deformation and resolved volumetric changes in two distinct subsurface regions beneath Lusi as well as a region beneath the nearby Wunut gas field. The ground deformation associated with Lusi results from the withdrawal of mud from the UKF as well as the withdrawal of fluids from >3500 m depth, with a centroid around 4300 m depth. This deep fluid source is consistent with the inferred source depth of hydrocarbons erupting at Lusi [*Mazzini et al*., 2012] and indicates that gas and fluids may be migrating from >4 km depth on eruptive timescales. We find that the ratio of volume change rate in the shallow source to that in the deep source is in general agreement with trends of decreasing water content since the initiation of the eruption in May 2006. Finally, we find evidence for lateral expansion of the mud source during May 2006 and early 2007. This expansion due to progressive mobilization of mud was suggested on theoretical grounds by *Rudolph et al*. [2011].

Acknowledgments

The interferograms used in this study were generated using the GMTSAR software [*Sandwell et al*., 2011]. Radar data are provided through Alaska SAR Facilities. We thank the reviewers and editor for their constructive comments. Shirzaei and Manga thank support from National Science Foundation grant EAR-1344441. To obtain copy of the InSAR deformation time series and model results, contact the author at shirzaei@asu.edu.

The Editor thanks two anonymous reviewers for their assistance in evaluating this paper.

References

Abidin, H. Z., R. J. Davies, M. A. Kusuma, H. Andreas, and T. Deguchi (2009), Subsidence and uplift of Sidoarjo (East Java) due to the eruption of the Lusi mud volcano (2006–present), *Environ. Geol.*, *57*(4), 833–844, doi:10.1007/s00254-008-1363-4.

Aoki, Y., and T. P. Sidiq (2014), Ground deformation associated with the eruption of Lumpur Sidoarjo mud volcano, east Java Indonesia, *J. Volcanol. Geotherm. Res.*, *278*, 96–102, doi:10.1016/j.jvolgeores.2014.04.012.

Bjerhammar, A. (1973), *Theory of Errors and Generalized Matrix Inverse*, pp. 127–128, Elsevier, Amsterdam.

Chen, C. W., and H. A. Zebker (2001), Two-dimensional phase unwrapping with use of statistical models for cost functions in nonlinear optimization, *J. Opt. Soc. Am. A.*, *18*, 338–351.

Costantini, M., and P. A. Rosen (1999), A generalized phase unwrapping approach for sparse data, paper presented at the IEEE 1999 International Geoscience and Remote Sensing Symposium (IGARSS), Hamburg, Germany.

D'Auria, L., F. Giudicepietro, M. Martini, and R. Lanari (2012), The 4D imaging of the source of ground deformation at Campi Flegrei caldera (southern Italy), *J. Geophys. Res.*, *117*, B08209, doi:10.1029/2012JB009181.

Davies, R., M. Manga, M. Tingay, and R. Swarbrick (2011), Fluid transport properties and estimation of overpressure at the Lusi mud volcano, East Java Basin (Tanikawa et al., 2010), *Eng. Geol.*, *121*(1–2), 97–99, doi:10.1016/j.enggeo.2011.03.010.

Farr, T. G., et al. (2007), The Shuttle Radar Topography Mission, *Rev. Geophys.*, *45*, RG2004, doi:10.1029/2005RG000183.

Franceschetti, G., and R. Lanari (1999), *Synthetic Aperture Radar Processing*, CRC Press, Boca Raton, Fla.

Fukushima, Y., J. Mori, M. Hashimoto, and Y. Kano (2009), Subsidence associated with the LUSI mud eruption, East Java, investigated by SAR interferometry, *Mar. Pet. Geol.*, *26*(9), 1740–1750, doi:10.1016/j.marpetgeo.2009.02.001.

Grewal, M. S., and A. P. Andrews (2001), *Kalman Filtering: Theory and Practice Using MATLAB*, 416 pp., Wiley-Interscience, Hoboken, N. J.

Harris, R., and P. Segall (1987), Detection of a locked zone at depth on the Parkfield, California segment of the San Andreas fault, *J. Geophys. Res.*, *92*, 7945–7962, doi:10.1029/JB092iB08p07945.

Istadi, B. P., G. H. Pramono, P. Sumintadireja, and S. Alam (2009), Modeling study of growth and potential geohazard for LUSI mud volcano: East Java, Indonesia, *Mar. Pet. Geol.*, *26*(9), 1724–1739, doi:10.1016/j.marpetgeo.2009.03.006.

Kusumastuti, A., P. Van Rensbergen, and J. K. Warren (2002), Seismic sequence analysis and reservoir potential of drowned Miocene carbonate platforms in the Madura Strait, East Java, Indonesia, *AAPG Bull.*, *86*(2), 213–232.

Lupi, M., E. H. Saenger, F. Fuchs, and S. A. Miller (2014), Corrigendum to Lusi mud eruption triggered by geometric focusing of seismic waves, *Nat. Geosci.*, *7*(9), 687–688, doi:10.1038/ngeo2239.

Marshall, J., and J. Bethel (1996), Basic concepts of L1 norm minimization for surveying applications, *J. Surv. Eng.*, *122*(4), 168–179.

Massonnet, D., M. Rossi, C. Carmona, F. Adragna, G. Peltzer, K. Feigl, and T. Rabaute (1993), The displacement field of the Landers earthquake mapped by radar interferometry, *Nature*, *364*, 138–142.

Masterlark, T., and Z. Lu (2004), Transient volcano deformation sources imaged with interferometric synthetic aperture radar: Application to Seguam Island, Alaska, *J. Geophys. Res.*, *109*, B01401, doi:10.1029/2003JB002568.

Mazzini, A., H. Svensen, G. G. Akhmanov, G. Aloisi, S. Planke, A. Malthe-Sørenssen, and B. Istadi (2007), Triggering and dynamic evolution of the LUSI mud volcano, Indonesia, *Earth Planet. Sci. Lett.*, *261*(3–4), 375–388, doi:10.1016/j.epsl.2007.07.001.

Mazzini, A., A. Nermoen, M. Krotkiewski, Y. Podladchikov, S. Planke, and H. Svensen (2009), Strike-slip faulting as a trigger mechanism for overpressure release through piercement structures: Implications for the Lusi mud volcano, Indonesia, *Mar. Pet. Geol.*, *26*(9), 1751–1765, doi:10.1016/j.marpetgeo.2009.03.001.

Mazzini, A., G. Etiope, and H. Svensen (2012), A new hydrothermal scenario for the 2006 Lusi eruption, Indonesia: Insights from gas geochemistry, *Earth Planet. Sci. Lett.*, *317*, 305–318, doi:10.1016/j.epsl.2011.11.016.

Mikhail, E. M. (1976), *Observations and Least Squares*, 497 pp., IEP, New York.

Mossop, A., and P. Segall (1999), Volume strain within the Geysers geothermal field, *J. Geophys. Res.*, *104*(B12), 29,113–29,131, doi:10.1029/1999JB900284.

Pascal, K., J. Neuberg, and E. Rivalta (2014), On precisely modelling surface deformation due to interacting magma chambers and dykes, *Geophys. J. Int.*, *196*(1), 253–278, doi:10.1093/gji/ggt343.

Richards, J. R. (2011), Report into the past, present, and future social impacts of Lumpur Sidoarjo, *Rep.*, Humanitus Sidoarjo Fund.

Rudolph, M. L., and M. Manga (2010), Mud volcano response to the 4 April 2010 El Mayor-Cucapah earthquake, *J. Geophys. Res.*, *115*, B12211, doi:10.1029/2010JB007737.

Rudolph, M. L., L. Karlstrom, and M. Manga (2011), A prediction of the longevity of the Lusi mud eruption, Indonesia, *Earth Planet. Sci. Lett.*, *308*(1–2), 124–130, doi:10.1016/j.epsl.2011.05.037.

Rudolph, M. L., M. Shirzaei, M. Manga, and Y. Fukushima (2013), Evolution and future of the Lusi mud eruption inferred from ground deformation, *Geophys. Res. Lett.*, *40*, 1089–1092, doi:10.1002/grl.50189.

Sandwell, D., R. Mellors, X. Tong, M. Wei, and P. Wessel (2011), Open radar interferometry software for mapping surface deformation, *Eos Trans. AGU*, *92*(28), doi:10.1029/2011EO280002.

Segall, P. (2010), *Earthquake and Volcano Deformation*, 458 pp., Princeton Univ. Press, Princeton, N. J.
Shirzaei, M. (2013), A wavelet-based multitemporal DInSAR algorithm for monitoring ground surface motion, *IEEE Geosci. Remote Sens. Lett.*, *10*(3), 456–460, doi:10.1109/Lgrs.2012.2208935.
Shirzaei, M., and R. Bürgmann (2012), Topography correlated atmospheric delay correction in radar interferometry using wavelet transforms, *Geophys. Res. Lett.*, *39*, L01305, doi:10.1029/2011GL049971.
Shirzaei, M., and T. R. Walter (2010), Time-dependent volcano source monitoring using interferometric synthetic aperture radar time series: A combined genetic algorithm and Kalman filter approach, *J. Geophys. Res.*, *115*, B10421, doi:10.1029/2010JB007476.
Shirzaei, M., and T. R. Walter (2011), Estimating the effect of satellite orbital error using wavelet based robust regression applied to InSAR deformation data, *IEEE Trans. Geosci. Remote Sens.*, *49*(1), 4600–4605.
Tingay, M. (2015), Initial pore pressures under the Lusi mud volcano, Indonesia, *Interpretation*, *3*(1), SE33–SE49, doi:10.1190/INT-2014-0092.1.
Tingay, M., O. Heidbach, R. Davies, and R. Swarbrick (2008), Triggering of the Lusi mud eruption: Earthquake versus drilling initiation, *Geology*, *36*(8), 639–642, doi:10.1130/g24697a.1.
Tingay, M., M. L. Rudolph, M. Manga, R. Davies, and C.-Y. Wang (2015), Initiation of the Lusi mudflow disaster, *Nat. Geosci.*, *8*, 493–494, doi:10.1038/ngeo2472.
Vanderkluysen, L., M. R. Burton, A. B. Clarke, H. E. Hartnett, and J.-F. Smekens (2014), Composition and flux of explosive gas release at LUSI mud volcano (East Java, Indonesia), *Geochem. Geophys. Geosyst.*, *15*, 2932–2946, doi:10.1002/2014GC005275.
Vasco, D. W., L. R. Johnson, and N. E. Goldstein (1988), Using surface displacement and strain observations to determine deformation at depth, with an application to Long Valley Caldera, California, *J. Geophys. Res.*, *93*(B4), 3232–3242, doi:10.1029/JB093iB04p03232.
Vasco, D. W., C. Wicks, K. Karasaki, O. Marques, and J. B. Hulen (2002), Geodetic imaging: Reservoir monitoring using satellite interferometry, *Geophys. J. Int.*, *149*(3), 555–571, doi:10.1046/j.1365-246X.2002.01569.x.